TISSUE ENGINEERING: Part C
Volume 25, Number 1, 2019
© Mary Ann Liebert, Inc.
DOI: 10.1089/ten.tec.2018.0307

termis
Tissue Engineering
& Regenerative Medicine
International Society

METHODS ARTICLE

Multimaterial Segmented Fiber Printing for Gradient Tissue Engineering

Luis Diaz-Gomez, PhD,[1–3] Brandon T. Smith, BS,[1–4] Panayiotis D. Kontoyiannis,[1–3] Sean M. Bittner, BS,[1–3] Anthony J. Melchiorri, PhD,[1–3] and Antonios G. Mikos, PhD[1–3]

In this work, we present a printing method to fabricate scaffolds consisting of multimaterial segmented fibers. Particularly, we developed a reproducible printing process to create single fibers with multiple discrete compositions and control over the distribution of particulate ceramics—namely hydroxyapatite (HA) and β-tricalcium phosphate (TCP)—within poly(ε-caprolactone)-based composite scaffolds. Tensile testing revealed that the mechanical integrity of individual segmented fibers was preserved compared with nonsegmented fibers, and microcomputed tomography and thermal analysis confirmed the homogeneous distribution of ceramics incorporated in the fiber compositions. Moreover, we printed and characterized composite scaffolds containing model inverse radial gradients of HA and TCP that could serve as a tunable platform to control the degradation rate of the scaffolds and match bone tissue ingrowth. The morphology of the gradient scaffolds was assessed, and their bulk compressive mechanical properties were found to be in the same range as human trabecular bone. Finally, scaffold degradation was monitored for up to 10 weeks in phosphate-buffered saline pH 7.4 and 0.1 M HCl solution, and scaffolds containing TCP in their composition showed increased degradation compared with those containing HA. This work provides a new methodology for the fabrication and characterization of porous scaffolds containing designer composition gradients that could serve as a platform for the preparation of complex scaffolds for tissue engineering applications.

Keywords: 3D printing, scaffold design, bone tissue engineering, biofabrication, multimaterial printing, graded scaffolds

Impact Statement

This study introduces a segmented three-dimensional printing methodology to create multimaterial porous scaffolds with discrete gradients and controlled distribution of compositions. This methodology can be adapted for the preparation of complex, multimaterial scaffolds with hierarchical structures and mechanical integrity useful in tissue engineering.

Introduction

Current treatment paradigms for bone loss have historically been limited by nondegradability, stiffness, and lack of integration into host tissue.[1,2] However, continued advances in tissue engineering techniques are enabling researchers to address these limitations. Such strategies require the development of a key component to induce tissue regeneration: a biomaterial-based scaffold.[3,4] These scaffolds must be fabricated in a manner that meets certain criteria specific to tissue type and location, including mechanical properties, biocompatibility, biodegradability, and micro- and macroarchitecture matching the target tissue.[5] For example, to treat a critical-sized bone defect, a scaffold must degrade at a rate that matches tissue ingrowth, remain strong enough for use in weight-bearing areas, and promote new bone formation.[6,7] Furthermore, scaffolds for bone regeneration should present an interconnected porous structure that mimics the porosity inherent in native bone tissue, with osteoconductive moieties that support mineralization.[8] Porosity in these scaffolds is crucial, as pores allow migration and proliferation of cells and improve

[1]Department of Bioengineering, BioScience Research Collaborative, Rice University, Houston, Texas.
[2]Biomaterials Lab, Rice University, Houston, Texas.
[3]NIH/NIBIB Center for Engineering Complex Tissues.
[4]Medical Scientist Training Program, Baylor College of Medicine, Houston, Texas.

vascularization.[9] In addition, bone tissue, as in other complex tissues, presents a graded compositional structure with varied mechanical behavior; it is mandatory to match mechanical properties of the porous scaffold design with the host tissue structure to avoid failure of the implant due to collapse of the structure or marginal resorption.[5,10,11] As mentioned above, any tissue-engineered scaffold should degrade at a rate matching the formation of new tissue. However, the actual behavior seen in previous works is that scaffolds often undergo degradation at rates that are either too slow or too fast, leading to implant failure or incomplete regeneration.[12]

Recent advances in biofabrication methodologies have enabled the preparation of bioresorbable, porous scaffolds for bone regeneration. Yet, many of these approaches often cannot accurately replicate the intricate structural and compositional gradients present in bone tissue.[12,13] Recently, several techniques have been used to develop vertical and horizontal gradients that can mimic complex gradients found in native tissues such as osteochondral defects or tendon-to-bone insertions.[14–17] Despite good results for these gradients, the preparation of complex multimaterial scaffolds with precise structures is still immature in development. There is a lack of methodologies to efficiently generate scaffolds with tailored three-dimensional (3D) control over distributions in composition, structure, degradation rate, and morphological and mechanical properties. Methods such as solvent casting, freeze-drying, phase separation, and rapid prototyping have been used alone or in combination, but they often yield scaffolds with poor mechanical properties, a lack of controlled and interconnected porous structures, and inadequate structural integrity between the different compositions.[12] In particular, the most common 3D printing methodologies to create such structures rely on the extrusion of biomaterials in fiber-based structures. However, 3D-printed gradients and multimaterial prints with these techniques may experience issues such as delamination and poor material interfaces, compromising the mechanical integrity of the structures.[18,19] Despite previous efforts with the development of platforms to create gradients in single hydrogel fibers,[20] it is generally not possible in most 3D printing configurations to print a gradient of discrete variations of materials in a single, continuous fiber, limiting a user's control over complex scaffold designs.

Since bone is a composite formed mainly of collagen as an organic phase and hydroxyapatite (HA) as an inorganic phase, polymer/ceramic composites present a possible candidate for mimicking this structure. To provide the mechanical properties necessary for a bone scaffold, biocompatible synthetic polymers such as poly(ε-caprolactone) (PCL), poly(L-lactic acid) (PLLA), or the copolymer poly(D,L-lactic-co-glycolic acid) (PLGA) are often used in lieu of collagen in the organic phase.[21] These materials are known for their slow hydrolytic degradation and the ease of use for fabricating 3D scaffolds with high reproducibility. To emulate the inorganic phase, composite scaffolds are mainly prepared with ceramics such as HA, which has the strength to be used in weight-bearing bones but is only slightly biodegradable, and β-tricalcium phosphate (TCP), which is more biodegradable but less mechanically robust.[22,23] The incorporation of ceramics has been reported to buffer the pH of the environment surrounding the implant and prevent adverse reactions such as inflammation, while enhancing osteoconductivity and thus new bone formation. Compared with using either ceramics or synthetic polymers alone, composite scaffolds have been shown to have a synergistic, positive effect on bone regeneration.[24,25]

In this work, we aimed to develop a 3D printing method to build porous multimaterial scaffolds by creating fibers composed of segments from unique compositions that can be used on standard multihead 3D printing configurations. We then used the printing methodology to prepare scaffolds containing inverse radial gradients of HA (higher in the core) and TCP (higher in the outer ring) to create composite scaffolds with tunable degradative and compressive properties and osteoconductive factors while maintaining a highly interconnected porous structure. Printing reproducibility and homogeneous dispersion of ceramics throughout the printed constructs were assessed, the structures of printed scaffolds were characterized, and the morphological and mechanical integrity of extruded fibers was evaluated. Finally, the degradation kinetics of scaffolds was assessed under physiological and accelerated conditions.

Materials and Methods

Materials

Powdered PCL (nominal molecular weight 50,000 Da) was obtained from Polysciences (Warrington, PA). Nanohydroxyapatite (average particle size 208 nm), HA (average particle size 880 nm; used to validate the particle distribution using microcomputed tomography [microCT]), and β-TCP (average particle size 130 nm) were from Sigma-Aldrich (St. Louis, MO).

Scaffold printing

Powdered HA and TCP were homogeneously mixed with PCL in different proportions (Table 1) using a mortar and pestle. The powdered mixtures were placed in metal cartridges, heated to 160°C, and extruded through a 22G blunt needle (0.4 mm inner diameter) using a commercial 3D printing system (3D Bioplotter; EnvisionTEC, Gladbeck, Germany). To create computer models for printing, cylindrical scaffolds of 10 mm in diameter and 5 mm height were designed in SketchUp (Trimble, Sunnyvale, CA) and sliced into 16 layers (0.32 mm slicing thickness) using BioplotterRP software (EnvisionTEC). A filling pattern was created by drawing parallel straight strands with a 0.4 mm on-center spacing. Homogeneous scaffolds (PCL, PCL-HA30, PCL-TCP30, and PCL-HA15TCP15) were printed from a single cylindrical model, while gradient scaffolds (core: PCL-HA30; middle ring: PCL-HA15TCP15; outer ring: PCL-TCP30) were printed as three concentric rings with 0.4 mm of overlap between each ring, as shown in Figure 1. Printing conditions (pressure, speed, pre- and postflow) were set for each condition based on preliminary studies to obtain fibers with a similar, consistent diameter of *ca.* 480 μm, and are shown in Table 1. Printing pattern consisted of parallel strands with 0.6 mm on-center spacing. Fiber orientation of each new layer was perpendicular to the previous layer. The ceramic content in the scaffolds (30 wt%) was set after preliminary studies and was chosen as it was the highest ceramic/polymer ratio capable of being printed in a reproducible manner. In parallel, we also prepared a graded scaffold

Table 1. Composition and Printing Conditions of Composite Scaffolds

Scaffold	*PCL (wt%)*	*HA (wt%)*	*TCP (wt%)*	*Pressure (bar)*	*Speed (mm/s)*	*Preflow (s)*	*Postflow (s)*
PCL	100	0	0	5.0	1.2	0.2	0.3
PCL-HA30	70	30	0	5.7	0.5	0.3	0.3
PCL-TCP30	70	0	30	5.5	0.8	0.2	0.3
PCL-HA15TCP15	70	15	15	5.7	0.7	0.3	0.3
Gradient							
Core							
PCL-HA30	70	30	0	5.5	0.5	0.6	0.5
Middle ring							
PCL-HA15TCP15	70	15	15	5.7	0.7	0.5	0.7
Outer ring							
PCL-TCP30	70	0	30	5.7	0.8	0.5	0.5

HA, hydroxyapatite; PCL, poly(ε-caprolactone); TCP, tricalcium phosphate.

composed of PCL-HA30 in the core, PCL-HA15 in the middle ring, and only PCL in the outer ring, as a proof-of-concept composition to show through microCT analysis the presence of different concentrations of HA within the scaffold.

Validation of the developed printing methodology

The structure and HA distribution of the composite scaffolds printed as one continuous fiber or in segments were analyzed using microCT. Briefly, samples ($n = 3$) from all experimental groups were scanned using a SkyScan 1272 X-ray Micro-CT (Bruker, Kontich, Belgium). Images were obtained by 180° scanning at 7 μm/pixel resolution with Al 0.25 nm filter at voltage and current settings of 60 kV and 166 mA, respectively. Scan images were reconstructed, resliced, and analyzed using NRecon and CTAn software provided by Bruker. For porosity and pore interconnectivity analyses, the scanned object volumes were converted into binary images using a threshold of 38–255 for PCL and 80–255 for the ceramic. MicroCT scans were also used to evaluate the dispersion of ceramics within the scaffolds and, especially, the presence of aggregates that could compromise the homogeneous distribution of the ceramic phase in the scaffold structure. Since the resolution used to scan the samples was significantly larger than the average particle size of the nanosized HA and TCP used for preparation of composite scaffolds, we selected HA with a higher particle size (880 nm) to assess the distribution using microCT.

To evaluate the binding regions of the fibers printed in segments, scaffolds were sputter coated with gold and imaged using scanning electron microscopy (SEM) (Quanta 400 ESEM FEG; FEI, Hillsboro, OR). Samples were imaged under high vacuum at 10 kV and different magnifications.

To evaluate the effect of printing methodology and the compositional gradient on the mechanical properties of the scaffold, tensile testing was performed. The tensile properties of the printed fibers were assessed by first using the printing methodologies described above to print single fibers instead of full scaffolds. Briefly, individual fibers, 15 mm in length, of PCL, PCL-HA30, PCL-TCP30, and PCL-HA15TCP15 were printed as one or three segments with gradients. Fibers consisted either of one continuous fiber of a single material or a three-segmented fiber. Segmented fibers were created using the overlapping printing methodology as described above. Examining the tensile strength of the overlapping segments within composite and gradient fibers was crucial to validating the maintenance of mechanical integrity during the described printing process. Thus, these segmented fibers enabled the testing of the joined regions of composed material fibers to determine whether they retained the tensile strength of single fibers. Tensile strength was measured using an Enduratec ELF 3200 tensile bench (Bose, Framingham, MA) and evaluated at 1 mm/s until 20% strain to determine elastic moduli according to ASTM D638-14 for reinforced and unreinforced plastics.

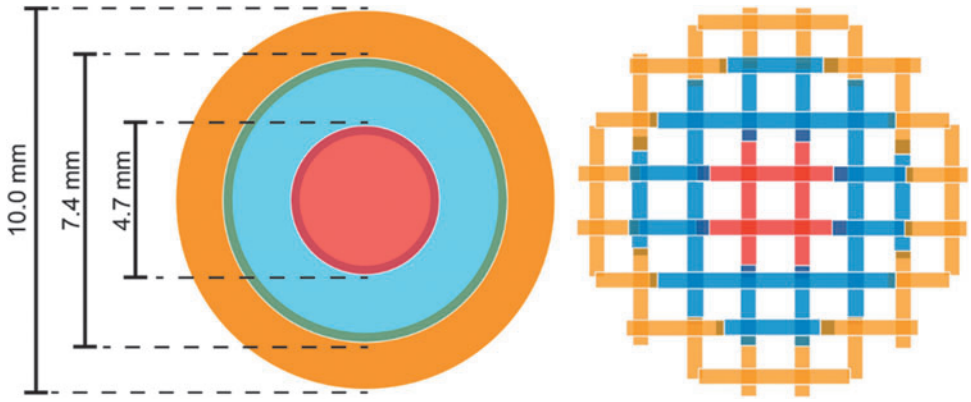

FIG. 1. 3D model (*left*) and filling pattern (*right*) of the radial gradient composite scaffolds. *Orange*, *blue* and *red* colors represent different compositions (e.g., PCL-TCP30 in *orange*, PCL-HA15TCP15 in *blue*, and PCL-HA30 in *red*). 3D, three dimensional; PCL, poly(ε-caprolactone).

Differential scanning calorimetry

Differential scanning calorimetry was carried out using a DSC-Q100 (TA Instruments, New Castle, DE) under a nitrogen gas flow of 50 mL/min at a heating rate of 10°C/min in the 0–120°C range. Degree of PCL crystallinity (in percentage) was calculated as in Equation (1):

$$\text{Crystallinity } (\%) = \frac{\Delta H_m}{\chi \cdot \Delta H^{\circ}_{m\,\text{PCL}}} \times 100 \qquad (1)$$

where χ represents the weight fraction of PCL in the sample; ΔH_m, the melting enthalpy of the sample; and $\Delta H^{\circ}_{m\,\text{PCL}}$, the melting enthalpy of 100% crystalline PCL (142 J/g).[26]

Advanced polymer chromatography

The molecular weight of the PCL before and after printing was determined using an ACQUITY Advanced Polymer Chromatography system (Waters, Milford, MA), which consisted of a pump (ACQ-ISM), sample manager (ACQ-FTN), column manager (ACQ-CM), and refractive index detector (ACQ-RI). Samples ($n=3$) were fabricated using the conditions presented in Table 1. A small piece of the printed scaffold was cut such that each sample weighed 20 mg and then dissolved in 4 mL of tetrahydrofuran (THF) on a shaker table for 24 h. The resulting solution was filtered using 0.1 μm Acrodisc nylon syringe filters. Advanced polymer chromatography (APC) was performed at a flow rate of 0.5 mL/min with a Waters ACQUITY APC XT 125 2.5 μm 4.6×75 mm column at 35°C with the refractive index detector set at 45°C. Polystyrene standards ranging between 266 and 66,000 Da were used to construct a calibration curve. The number average molecular weight (M_n), weight average molecular weight (M_w), and polydispersity index were measured and calculated using Empower 3 (Waters).

Physical characterization of 3D scaffolds

Strand and pore size was evaluated by SEM. Scaffolds were sputter coated with gold and imaged using SEM (Quanta 400 ESEM FEG; FEI). Samples were imaged under high vacuum at 10 kV and different magnifications.

The porosity and interconnectivity of the composite scaffolds were analyzed using microCT. Briefly, samples ($n=5$) from all experimental groups were scanned using a SkyScan 1272 X-ray Micro-CT (Bruker). Images were obtained by using the same conditions described previously (Validation of the Developed Printing Methodology section). A volume of interest (VOI) of 5 mm diameter and 4 mm height was selected to analyze the porosity and interconnectivity of each sample. Interconnectivity is reported as the percentage of pore volume accessible from outside the VOI.

Thermogravimetric analysis

The ceramic content of the of the PCL-ceramic scaffolds was confirmed by thermogravimetric analysis (TGA) (TGA Q50; TA Instruments) following established methods.[27] Briefly, a 15 mg sample of printed material ($n=3$) was heated from 22°C to 95°C at a rate of 20°C/min. The temperature was then equilibrated at 100°C for 10 min followed by heating to 500°C at 20°C/min and was held for 10 min. Analysis was performed utilizing TA Universal Analysis (TA Instruments).

Mechanical property evaluation

The compressive strength and modulus of the composite scaffolds ($n=5$) were measured in a mechanical testing bench (10 kN load cell; 858 MiniBionixII®; MTS, Eden Prairie, MN) and calculated using the TestStar 790.90 mechanical data analysis package included in the manufacturer's software. Scaffolds were compressed perpendicularly to the printing plane at a crosshead speed of 1 mm/min after an initial preload of 25 N up to 20% strain. Stress/strain curves were calculated from the load versus displacement data using the initial external dimensions of each sample. The compressive strength of the structure was estimated as the maximum stress applied in each test.

Degradation analyses

Scaffolds of ~100 mg ($n=3$ per time point) were immersed in 5 mL of phosphate-buffered saline (PBS, pH 7.4) and incubated at 37°C for 10 weeks under constant movement using an orbital shaker (110 rpm). During the first week, PBS was changed every 24 h. Thereafter, PBS was changed weekly after pH measurement. At 2, 4, 6, 8, and 10 weeks, scaffolds were removed from PBS, washed with distilled water, and vacuum-dried for at least 24 h. Degradation rate was then calculated as shown in Equation (2):

$$\text{Mass loss } (\%) = \frac{M_i - M_f}{M_i} \times 100 \qquad (2)$$

In this equation, M_i and M_f represent the initial mass and final mass at each time point, respectively. In addition, scaffolds before and after degradation were dried at 37°C in vacuum for at least 24 h and analyzed by SEM using the conditions described previously to evaluate the effect of composition in the degradation of composites.

The degradation of composite scaffolds was also monitored in an acidic environment. Scaffolds of ~100 mg ($n=3$ per time point) were immersed in 5 mL 0.1 M HCl (pH 1.8) and maintained at 37°C for up to 10 weeks to recapitulate degradation of PCL *in vitro* at an accelerated rate as described previously.[28] For degradation in HCl, medium was changed every 24 h during the first week and then once per week until the end of the experiment. Since acidic degradation was expected to be faster than degradation in PBS, mass loss was monitored weekly during the first 4 weeks and then every 2 weeks up to 10 weeks. The initial and final mass of each scaffold was measured to calculate the mass loss as explained in the previous paragraph.

Statistical analysis

Statistics were analyzed using GraphPad Prism (GraphPad software, La Jolla, CA). All results are expressed as mean values with standard deviations. One-way analysis of variance (ANOVA) and Tukey's multiple comparison posttest were used. Differences were considered significant for $p<0.05$.

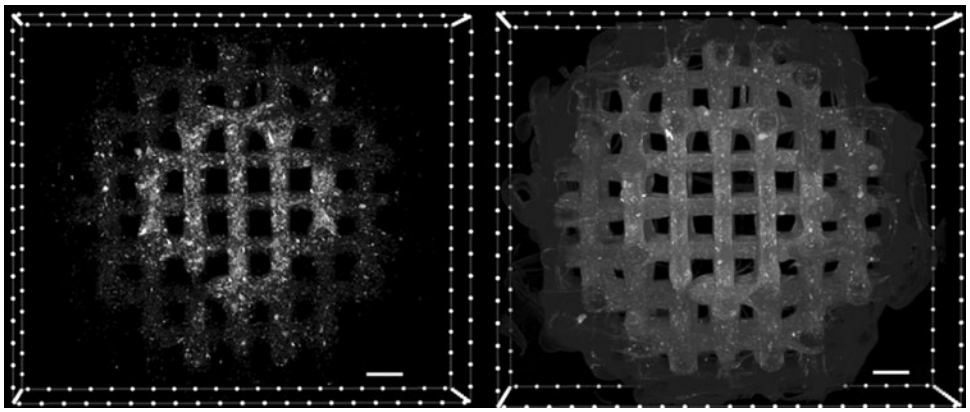

FIG. 2. Cross-sectional images of PCLHA30-PCLHA15-PCL gradient scaffolds prepared with micrometer HA. Images were generated from a 3D reconstruction of a microCT scan. *Left* image is an isolated view showing only the HA present within a scaffold and demonstrating the distribution of HA particles within the scaffold. *Right* image shows a transverse plane view of the scaffold. The images demonstrate the distribution of HA particles within the scaffold showing a higher concentration in the central region where HA concentration is intended to be higher (30 wt% HA, 70 wt% PCL), compared with the medial region (15 wt% HA, 85 wt% PCL), and no HA presence in the outer region (0 wt% HA, 100 wt% PCL). HA appears as opaque bright color compared with the *dark gray* PCL matrix. Scale bar = 500 μm. HA, hydroxyapatite; microCT, microcomputed tomography.

Results

Validation of the multimaterial segmented fiber printing methodology

The printing methodology described in this work enables the printing of segmented and graded composites within the same fibers and layers while maintaining the desired porosity. As shown in Figure 2, microCT analysis of the printed scaffolds confirmed a highly precise deposition of the different compositions within the same layer of the scaffolds. In the proof-of-concept design, a scaffold with three concentric regions containing graded HA concentrations (high, low, and no HA incorporation) was successfully printed. MicroCT reconstructions also showed that the HA content within each region is homogeneously distributed without any noticeable aggregation that could affect printing resolution or scaffold structure or as a result of sedimentation during the printing process. Furthermore, microCT analysis showed the high interconnection in the welding points between the different segments of each fiber.

The tensile properties of single fibers printed as one or three welded segments were measured to evaluate the effect of the printing method on the structural integrity of the fiber. The results are shown in Figure 3. We evaluated the effect of the incorporation of different ceramics in the composition (HA or TCP) to determine if the method is valid for different materials and particle sizes. There was no significant

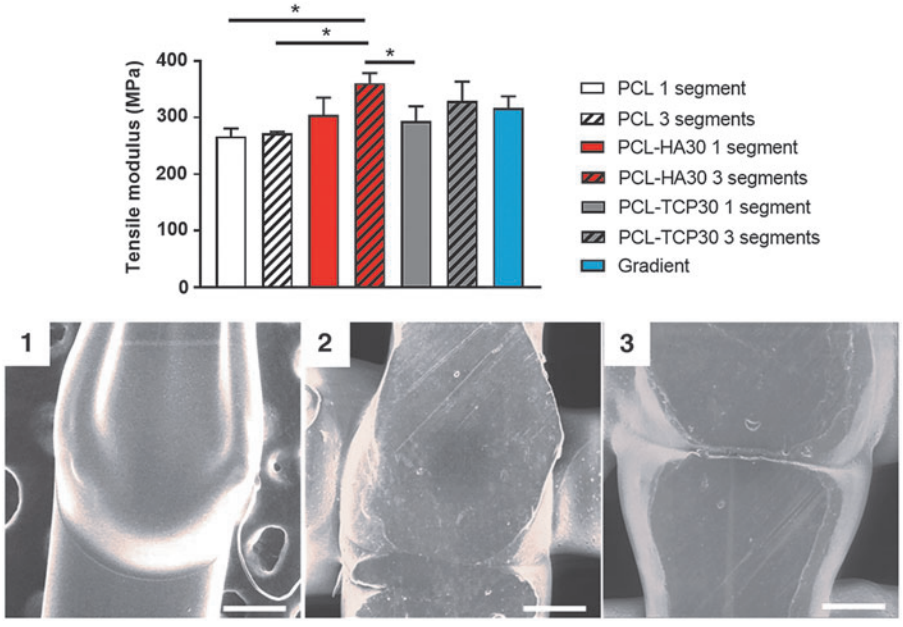

FIG. 3. *Above*: Tensile properties of single fibers printed in one or three segments. No statistical differences ($p > 0.05$) were found between fibers with the same composition printed as one or three segments ($n = 5$). However, the incorporation of ceramics (both HA and TCP) in the scaffold composition resulted in a significant increase in the tensile moduli of the fibers ($p < 0.05$, denoted by *asterisk*). *Below*: SEM micrographs highlighting the binding areas between different segments of single strands composed of PCL (1), PCL-HA30 (2), and PCL-TCP30 (3). Scale bar = 200 μm. SEM, scanning electron microscopy; TCP, tricalcium phosphate.

Table 2. Thermal Properties of Ceramic Scaffolds Before and After Printing ($N=3$)

	Preprinting		*Postprinting*	
Scaffold	*T_m (°C)*	*Crystallinity (%)*	*T_m (°C)*	*Crystallinity (%)*
PCL	61.2 ± 1.1	51.3 ± 2.2	64.1 ± 0.6[a]	45.7 ± 1.2
PCL-HA30	61.2 ± 1.0	51.7 ± 1.7	61.5 ± 1.0	54.7 ± 0.6[b]
PCL-TCP30	61.1 ± 0.7	51.8 ± 1.4	61.7 ± 0.8	49.8 ± 0.6[b]
PCL-HA15TCP15	61.5 ± 0.6	51.9 ± 2.0	61.7 ± 1.2	53.7 ± 2.8[b]

[a]Denotes statistical differences compared with preprinting.
[b]Denotes statistical differences compared with PCL postprinting scaffolds.

effect ($p<0.05$) on the tensile moduli of PCL fibers when printed continuously or in three segments. However, adding ceramics (HA or TCP) increased the tensile modulus of the fibers from 266.5 ± 13.8 MPa (PCL) to 304.7 ± 30.4 MPa (PCL-HA30) and 294.0 ± 25.9 MPa (PCL-TCP30). Similarly, fibers printed as three segments also revealed increased values of tensile moduli when ceramics were incorporated in the composition. Tensile modulus increased from 271.9 ± 3.0 MPa (PCL) to 360.8 ± 17.6 MPa (PCL-HA30), 328.6 ± 25.9 MPa (PCL-TCP30), and 317.0 ± 20.4 MPa (gradient). The compressive modulus of the composite scaffolds printed as one or three segments resulted in no significant differences, regardless of the composition and printing method (Supplementary Fig. S1; Supplementary Data are available online at www.liebertpub.com/tec).

Differential scanning calorimetry

Differential scanning calorimetry was carried out to evaluate the effect of the printing process and the incorporation of ceramics in the crystalline structure of PCL (Table 2). The incorporation of HA or TCP had no significant effect ($p<0.05$) on the melting temperature or crystallinity of PCL before printing. On the contrary, a significant increase in the melting temperature of PCL was shown after the printing process. Furthermore, PCL-ceramic scaffolds had a significantly higher crystallinity compared with PCL scaffolds after the printing process.

Advanced polymer chromatography

The number average molecular weight (M_n) and weight average molecular weight (M_w) of PCL present in the 3D composite scaffolds were evaluated by APC and the results are shown in Figure 4. The M_w of PCL in PCL-only and PCL-ceramic scaffolds was consistent at ~65,000 Da. Furthermore, the printing process had no significant effect ($p>0.05$) on the M_w in any of the studied groups. These results are similar to those obtained for the M_n of the PCL, which remained constant at ~57,000 Da in all groups before and after printing.

Pore and fiber morphology

The porous structure of the composite scaffolds was evaluated by microCT (Fig. 5 and Table 3). Homogeneous pore size and strand diameter distribution were shown in every condition regardless of the printing method used to build the scaffolds (continuous or segmental). The pore size and strand width of the composite scaffolds were not significantly different and were in the 510–560 and 430–500 μm range, respectively. The porosity of the scaffolds was also evaluated by microCT. Gradient scaffolds showed small prominences in the welding points between segments, but these had no effect on the total porosity of the scaffolds.

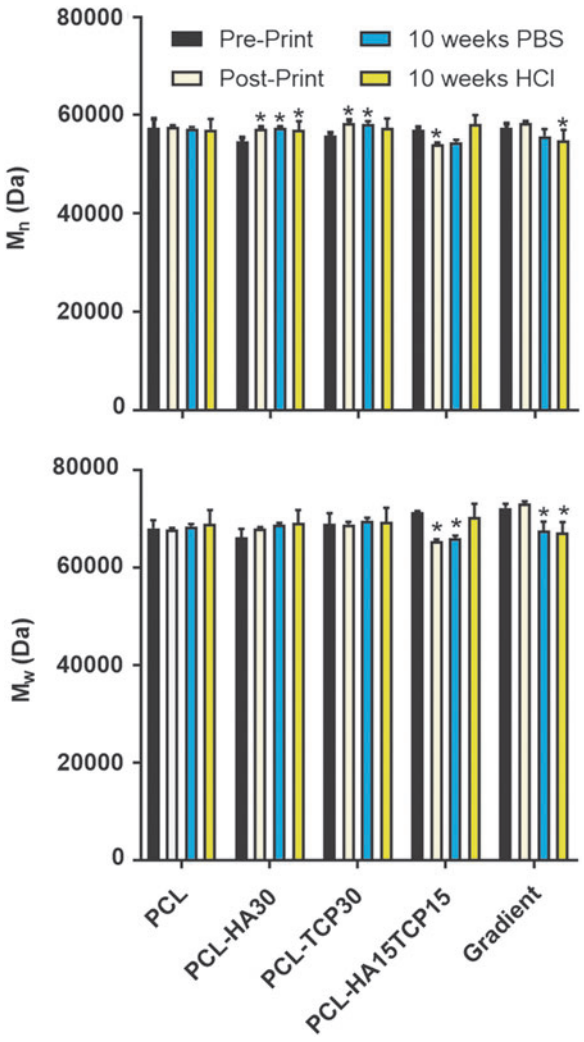

FIG. 4. **(A)** Number average molecular number (M_n) and **(B)** weight average molecular weight (M_w) of the PCL contained in the composite scaffolds evaluated by advanced polymer chromatography before and after the printing process and after 10 weeks of incubation in PBS (pH 7.4) or HCl (pH 1.8). *Mean statistical differences ($p<0.05$) compared with the preprinted scaffolds of each condition ($n=3$). PBS, phosphate-buffered saline.

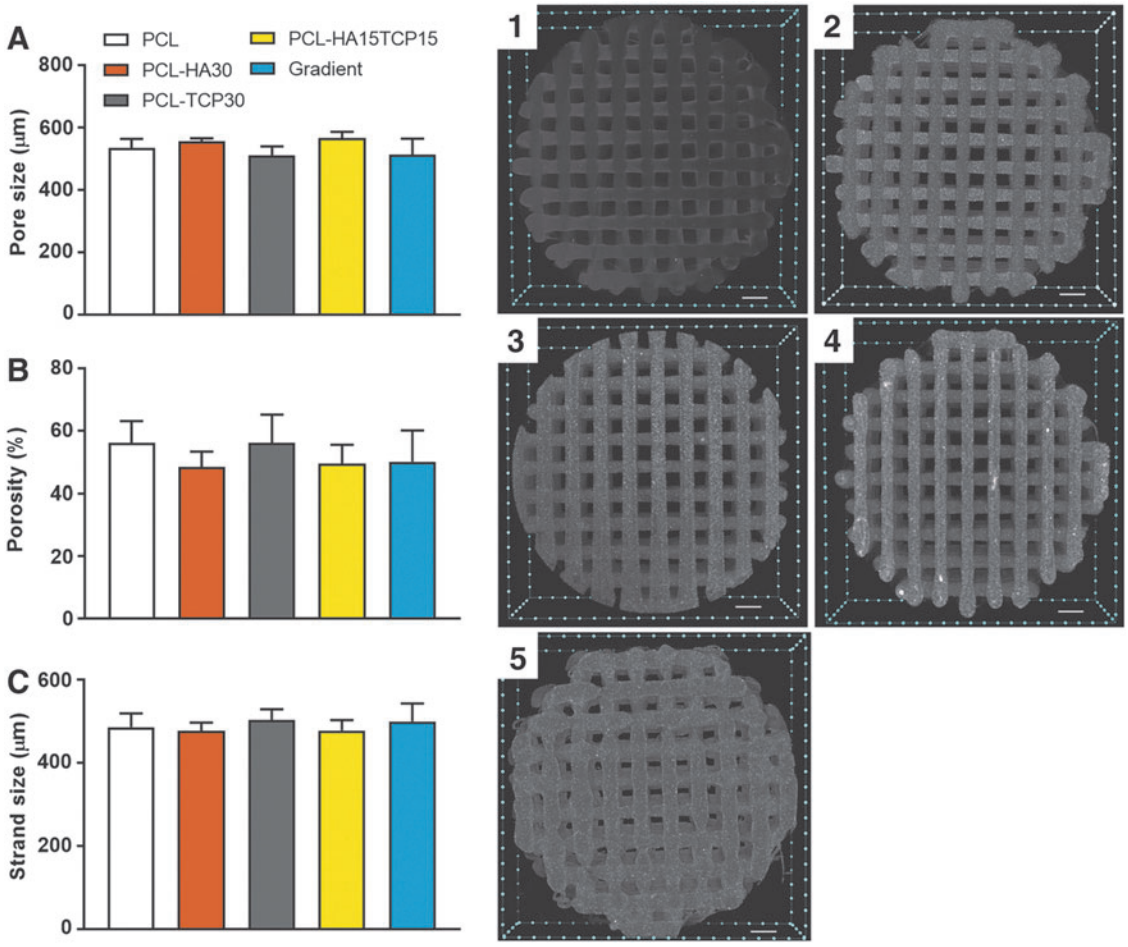

FIG. 5. *Left*: Pore size **(A)**, porosity **(B)**, and strand size **(C)** of the 3D composite scaffolds prepared with nanometer-sized ceramics and evaluated by microCT. Each composition is represented as mean ± standard deviation ($n = 5$). Pore and strand size results represent five scaffolds with 40 measurements per scaffold. *Right*: Transaxial images of PCL (1), PCL-HA30 (2), PCL-TCP30 (3), PCL-HA15TCP15 (4), and gradient (5). 3D composite scaffolds generated from a 3D reconstruction via microCT. Scale bar = 500 μm. Results show that the printing method and the composition do not affect the structure and morphology of the scaffolds.

All compositions showed a similar porosity of ~50% and the interconnectivity was close to 100% (threshold 7 μm). The microCT reconstructions revealed the presence of ceramics as homogeneous bright areas compared with the gray PCL scaffolds, which is due to the higher X-ray absorption of ceramics compared with organic compounds such as PCL. The absence of ceramic clumps can be explained by the nanometric particle size of both HA and TCP (~200 nm), which is four to five times smaller than the scanning threshold (700 nm).

Thermogravimetric analysis

The actual ceramic content of composite scaffolds was investigated by means of TGA and portions of different layers were chosen to confirm the homogeneity of the composition throughout the printing process (Table 3). Scaffolds composed of PCL-HA30, PCL-TCP30, PCL-HA15TCP15, and gradient were determined to have ceramic content of 31.0 wt%, 30.0 wt%, 30.4 wt%, and 30.3 wt%, respectively.

TABLE 3. STRUCTURAL CHARACTERIZATION ($N = 5$) AND CERAMIC CONTENT ($N = 3$) OF THE COMPOSITE THREE-DIMENSIONAL SCAFFOLDS

Scaffold	*Open porosity (%)*	*Closed porosity (%)*	*Pore size (μm)*	*Strand width (μm)*	*Ceramic content (%)*
PCL	51.5 ± 6.0	0.0 ± 0.0	534 ± 30	485 ± 34	0.0 ± 0.2
PCL-HA30	50.6 ± 5.7	0.0 ± 0.0	557 ± 9	432 ± 12	31.0 ± 0.6
PCL-TCP30	51.9 ± 6.4	0.0 ± 0.0	511 ± 29	502 ± 26	30.0 ± 0.7
PCL-HA15TCP15	49.4 ± 4.9	0.0 ± 0.0	567 ± 20	477 ± 25	30.4 ± 0.6
Gradient	47.0 ± 6.8	0.0 ± 0.0	513 ± 52	499 ± 43	30.3 ± 0.7

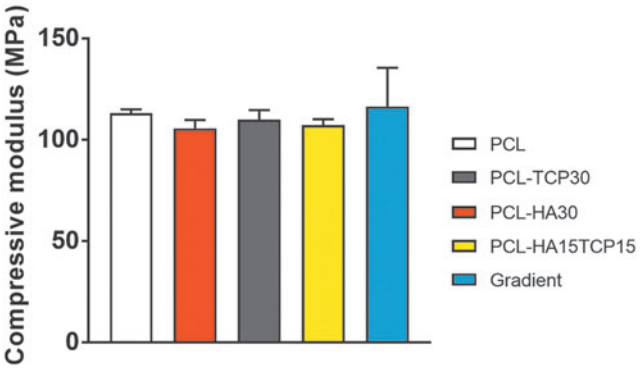

FIG. 6. Compressive modulus of composite 3D scaffolds. No statistical significances were found in the compressive modulus of the PCL and PCL-ceramic scaffolds. Data reported as mean ± standard deviations ($n = 5$ scaffolds).

Mechanical property evaluation

The compressive properties of the composite scaffolds were also carried out to evaluate the influence of ceramic addition to the composition of PCL scaffold (Fig. 6). All the compositions led to a similar compressive modulus in the 100–140 MPa range. No statistical differences were found between the compositions containing HA or TCP compared with the PCL control group.

Degradation studies

Figure 7A represents the mass loss of the composite scaffolds in time when incubated in PBS pH 7.4 at 37°C and 110 rpm oscillation. It was observed that during the first 8 weeks, mass loss represented less than 2% in all compositions. The pH values of the degradation buffer were measured (Fig. 8). After a slight decrease of the pH during the first week of incubation, pH was stabilized at 7.4 until the end of the experiment.

Figure 7B shows the mass loss of the composite scaffolds during their incubation in an acidic environment for accelerated degradation (HCl pH 1.8 at 37°C and 110 rpm oscillation), which is standard practice in studies where degradation time is projected to be extremely lengthy *in vitro* due to the degradation times of the materials used.[29] Scaffolds containing TCP showed a significant increase ($p < 0.05$) in their mass loss after the second week of incubation proportional to the content of TCP (PCL-TCP30>PCL-HA15TCP15) compared with the PCL and PCL-HA scaffolds. After 10 weeks, significant differences in mass loss were more evident depending on the composition of the samples. PCL-TCP30 scaffolds showed the highest degradation rate, with a 4.6% mass loss compared with the lowest rate, 1.3% shown by PCL scaffolds. PCL-HA15TCP15 showed 3.0% mass loss while gradient and PCL-HA30 scaffolds presented a similar degradation rate, with 2.0% mass loss.

M_n and M_w of PCL remaining in the scaffolds were evaluated after 10 weeks of incubation (Fig. 4). According to the mass loss results, there are significant differences in the M_n of the polymer after printing and incubation in PBS or acidic medium, compared with the preprinting group. However,

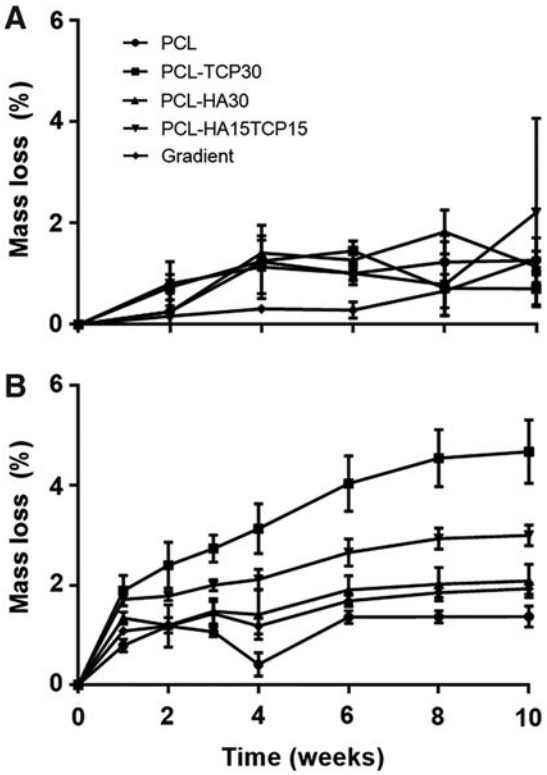

FIG. 7. Degradation profiles of the scaffolds after incubation during 10 weeks in PBS pH 7.4 **(A)** and in HCl pH 1.8 **(B)** at 37°C. Error bars denote standard deviation ($n = 3$).

the average PCL M_n decreased by less than 3% of the starting value. Regarding the M_w, no differences were found for PCL, PCL-TCP30, and PCL-HA30 scaffolds. However, a significant decrease in the M_w was found for PCL-HA15TCP15 and gradient scaffolds after incubation in PBS and acidic medium.

Figure 9 and Supplementary Figure S2 show the morphology of the surface of the scaffolds before and after immersion in acidic and PBS medium for 10 weeks. SEM analysis showed that no noticeable change to the surface of

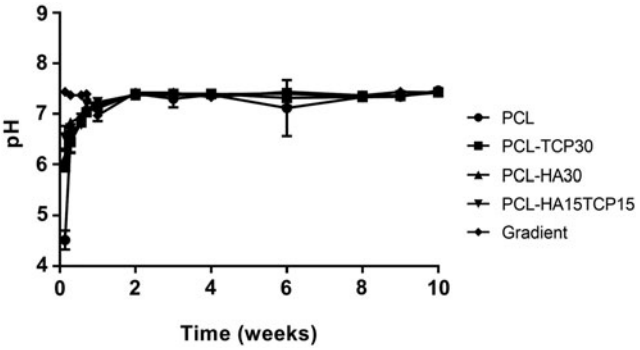

FIG. 8. Change in pH with time of PBS containing 3D composite scaffolds. Error bars denote standard deviation ($n = 3$).

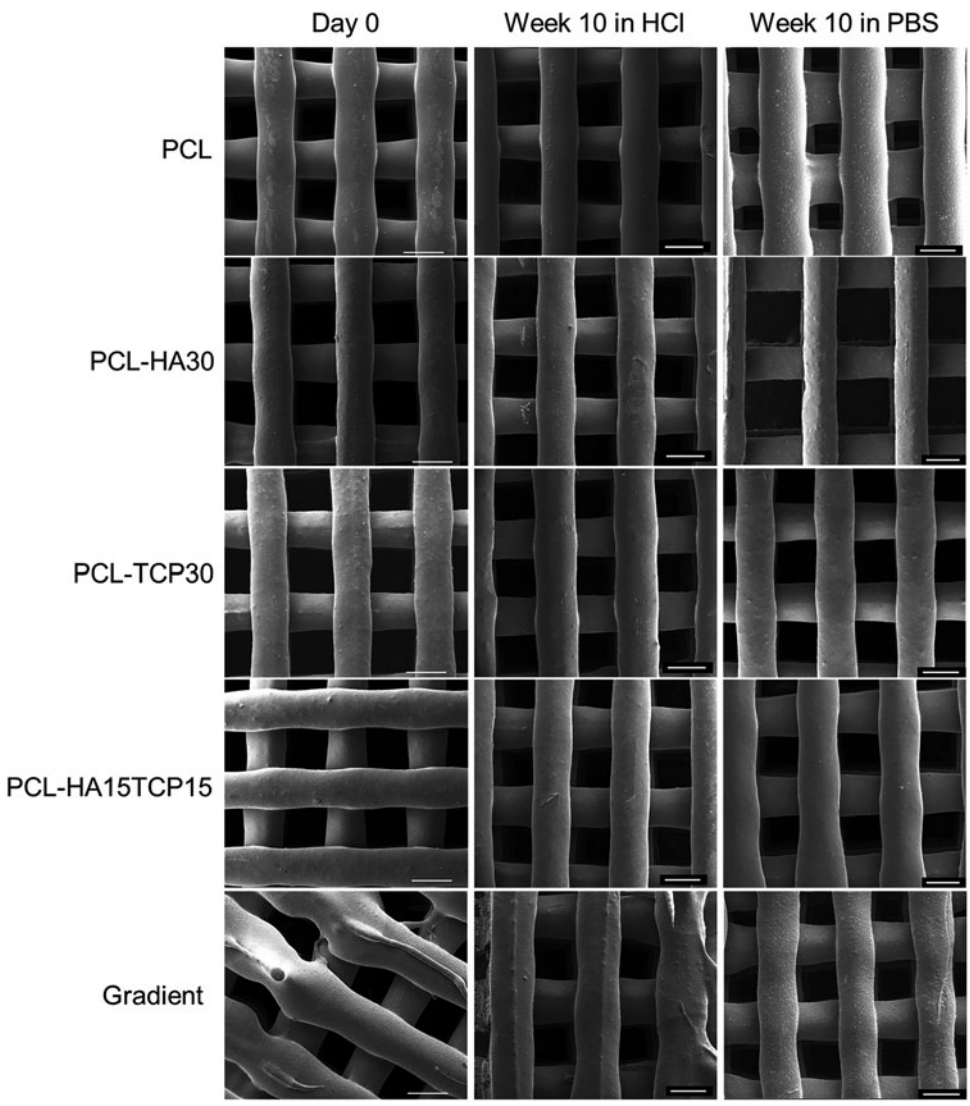

FIG. 9. Representative SEM images showing the superficial morphology of composite scaffolds on fabrication (day 0) and after immersion in HCl or PBS at 37°C for 10 weeks. Scale bar = 500 μm.

the scaffolds occurred during the degradation in both PBS and acidic medium.

Discussion

In this study, we developed a new 3D printing layer-by-layer methodology to prepare porous scaffolds consisting of segmented, multimaterial fibers while maintaining the structural and mechanical integrity of these individual fibers and the bulk scaffold.

The novelty of this work was the introduction of discrete compositions within the same fibers, and therefore, the same layers, avoiding weak interfaces between distinct material structures, while maintaining precise porous structure control. This methodology allowed for the deposition of different compositions within the same layer without compromising the structural or mechanical integrity of the scaffold as shown by tensile and imaging characterization. Contrary to what has been reported for scaffolds prepared using other techniques, nearly 100% of the pores in the scaffolds produced using this methodology were interconnected, which is crucial for tissue infiltration and secure graft fixation, allowing cell migration and exchange of nutrients and waste products from the ingrowing tissue during scaffold degradation.[30–32]

For this study, we selected PCL as the polymeric backbone since it is one of the most commonly used thermoplastic polymers for 3D printing due to its biocompatibility, biodegradability, strong mechanical properties, and regulatory history.[33] Theoretically, because the printing parameters used in this study are similar to conditions used in other thermoplastic polymers, this printing methodology could be applied to other polymers such as PLGA to prepare similar radially graded scaffolds.[27,34,35]

In this study, we have introduced potential bone graft substitutes with a designed graded composition that could serve as region-specific cues to provide biomimetic environments and cues to control properties such as mechanical and degradation properties, vascularization, and cell/material interactions.[17] The use of a 3D printer with three heads was essential to develop this methodology as it allowed the precise deposition of different compositions within the same method and avoided intricate setups. The success of this printing methodology is mainly shown by the results of the tensile modulus comparing that of the fibers printed as one segment and those printed in three segments. The similar

elastic behavior shown for all the compositions printed as one or three segments demonstrates that the welding of the different segments has no significant effect on the mechanical integrity of the fibers. We believe that these results can be explained because of the deliberate overlapping of segments. This may have been achieved by the remelting of the printed segment due to the high temperature of the newly extruded polymer and the metal needle. To take advantage of this, the most important part of this technique is that the length of the overlapping section must be equal to the diameter of the fiber. As shown in Figure 10, if the overlapping is shorter than the diameter of the extruded fiber (needle inner diameter), there will be less mixing between segments. This could potentially lead to a point of mechanical failure and, importantly, disrupt the precise morphology of the fiber, compromising fiber diameter uniformity. On the contrary, if one attempts to create an overlap larger than the diameter of the fiber, the morphology and reproducibility of a uniform fiber will also be compromised, disrupting reliable and predictable pore sizes. An adequate overlap preserves the mechanical integrity of a segmented fiber compared with an unsegmented fiber, while maintaining morphological consistency.

We evaluated the suitability of the developed printing methodology to prepare composite scaffolds with inverse radial gradients of HA and TCP to achieve tunable degradative properties that may be suitable for bone tissue engineering. It was hypothesized that the incorporation of an inverse radial gradient of HA (higher concentration in the core of the scaffold) and TCP (higher in the outer areas) would serve as a valid strategy to control the degradation rate of the scaffold. Furthermore, this inverse radial gradient of HA and TCP may enhance osseointegration while maintaining adequate mechanical properties for bone regeneration purposes in future research applications. The conventional techniques used to prepare scaffolds for bone and osteochondral regeneration such as solvent casting or gas foaming present some drawbacks, including lack of interconnectivity and control over the microarchitecture, along with the potential for hazardous residual porogens or solvents in the final structure.[30] Furthermore, with these methods, it is not possible to prepare scaffolds with composition or pore gradients. On the contrary, 3D printing has shown a great potential as a tool to precisely fabricate scaffolds with high interconnectivity and vertical composition and pore gradients that could be useful to replicate the intricate multilayer structure of the osteochondral tissue.[31,36,37] However, scaffolds with radial gradients have only been prepared by combining two or more fabrication techniques, such as 3D printing and solvent casting or freeze/drying or coextrusion, but the obtained scaffolds often lack interconnectivity, interphase integration, and adequate mechanical properties.[12,18,38]

Previous attempts to prepare multimaterial scaffolds useful in tissue engineering were based on coextrusion techniques that led to fibers with very limited morphology control and material distribution. For example, precise control over uniform pore size and interconnectivity can be inhibited by reliance on porogens or ratio of polymer/ceramic incorporated.[12,38] However, the method reported here is capable of preparing 3D constructs with very precise tunable structural properties, in terms of fiber deposition and structure, material distribution, and interconnectivity. Furthermore, the reported method allowed the preparation of composite scaffolds with homogeneous distribution using both nano- and micrometric ceramic particle sizes. Theoretically, it is possible not only to create radial or horizontal gradients but also vertical gradients to recapitulate complex compositional and structural properties found in tissues as this methodology is based on layer-by-layer deposition.

To obtain scaffolds with the same structural morphology, the printing method was tuned for each composition to print

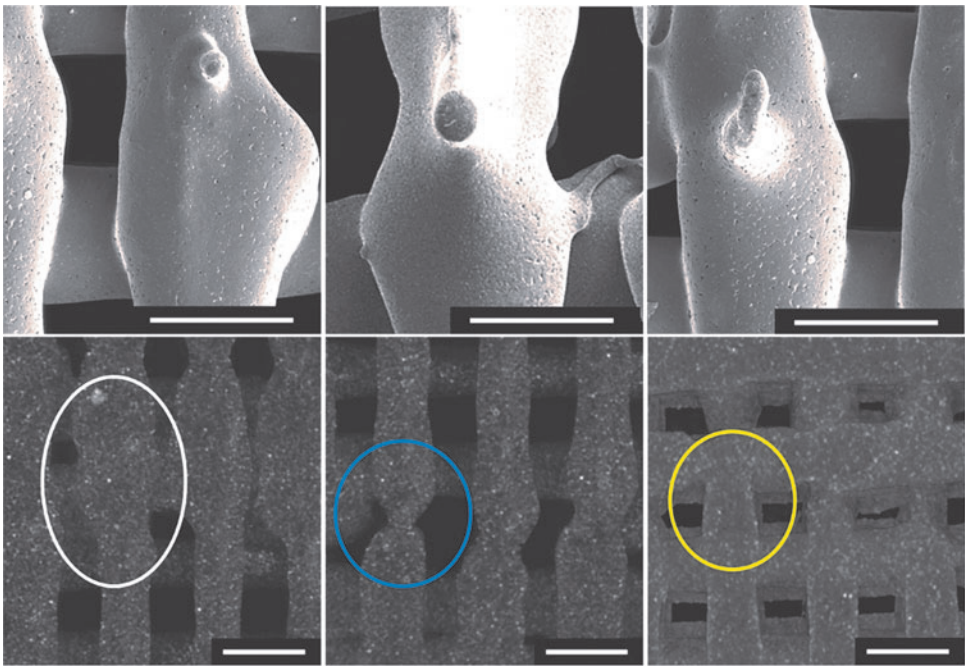

FIG. 10. SEM micrographs (*above*) and microCT reconstructions (*below*) of PCL-HA30 scaffolds highlighting an excessive (*left*), insufficient (*center*), and optimal (*right*) overlapping length. The *white circle* indicates an oversized structure as a result from an overlap larger than the diameter of the needle shown via microCT. The *blue circle* captures the neck produced by an overlap shorter than the diameter of the needle. The *yellow circle* indicates the defined structure of the fiber at the binding point when an overlap matching the inner diameter of the needle is applied. Scale bar = 500 μm.

scaffolds with similar pore and strand sizes. The content of HA and TCP (30 wt%) was selected after preliminary studies, as it was the highest content able to be included within PCL without compromising the architectural integrity of printed scaffolds using our Bioplotter 3D printer. We fabricated scaffolds with pores within the 400–500 μm range, reported to be adequate for the intended purpose of these scaffolds.[10] Regarding ceramic nanoparticle distribution, no aggregates bigger than 700 nm (threshold for microCT) were found in any of the compositions and evidenced by the low deviation of ceramic content shown after TGA analysis.

As shown in the thermal analyses, the incorporation of HA and TCP resulted in an increase in the crystallinity of the composite scaffolds after printing. Both HA and TCP particles acted as nucleation points, resulting in an increase in the crystal formation of the PCL during the cooling stage after printing.[39] Furthermore, according to molecular weights, the printing process did not result in significant degradation of PCL.

It has been reported that there is a reinforcement effect when HA or TCP is incorporated into polymeric matrices.[40] However, there was no significant difference in the compressive modulus between any of the composite scaffolds regardless of the composition, likely because of the high ceramic concentrations used in this study.[40,41] Furthermore, the values of compressive moduli obtained for all the printing conditions using this methodology were in the range of human trabecular bone (50–150 MPa).[30,42]

The addition of HA and TCP more so was hypothesized to accelerate the degradation of the scaffolds. During the standard degradation study, no significant differences were found in the degradation rate of the scaffolds from different compositions, as expected due to the low degradation rate of PCL, which is the main component of the scaffolds (70 wt%). Despite the degradation of PCL in acidic media being higher than in PBS under static conditions, 10 weeks might not be time enough to see a substantial mass loss when incubated at 37°C, as reported before.[43,44] Since ceramic nanoparticles are only physically blended to the backbone polymer and present high hydrophilicity, it is expected that after immersion in aqueous media, HA and TCP particles are solubilized because of their high surface area also depending on the solubility of the ceramic. Since TCP presents a higher solubility compared with HA, we believe that the regions of the gradient scaffolds where TCP is present will degrade faster than the HA regions for longer periods of degradation.[45] As shown in previous work, it is also expected that the extent of degradation and the differences between HA and TCP regions of the composite scaffolds after implantation will be greater than *in vitro* due to osteoclast resorption.[23,46,47]

Conclusions

In this work, we described and validated a new fabrication method to create multimaterial 3D scaffolds useful in tissue engineering by printing fibers composed of welded segments containing discrete polymer/ceramic compositions using a 3D printer with exchangeable heads. The fabrication method showed precise control over the deposition of fibers and circular scaffolds with three different compositions within the same layers being successfully printed. We confirmed the mechanical integrity of the segmented fibers by means of tensile testing and the content of ceramics by thermal analysis. Specifically, we printed and characterized composite scaffolds with inverse radial gradients of particulate HA and TCP using PCL as a backbone polymer that could serve as implants for bone regeneration with tunable degradation properties. The morphology and bulk mechanical properties of the scaffolds were also assessed. Compressive mechanical properties were found to be in the range of human trabecular bone. Furthermore, the process did not have any detrimental effect on the high interconnectivity of the scaffolds and no evident particle aggregation was found in any of the compositions. Finally, degradation was monitored for up to 4 months and, while macroscopic degradation was not relevant due to the low degradation rate of PCL *in vitro*, we showed significant degradation in regions where TCP was present in the composition. This methodology may be widely adapted to other 3D printing systems for the fabrication of complex tissue scaffolds.

Acknowledgments

This work was supported by the National Institutes of Health (P41 EB023833). L.D.-G. acknowledges Consellería de Cultura, Educación e Ordenación Universitaria, for a Postdoctoral fellowship (Xunta de Galicia, ED481B 2017/063). B.T.S. acknowledges the Baylor College of Medicine Medical Scientist Training Program. S.M.B. acknowledges the National Science Foundation Graduate Research Fellowship Program. We also acknowledge Shail Mehta from Rice University for his help assisting with the tensile tests.

Disclosure Statement

No competing financial interests exist.

References

1. Bose, S., Roy, M., and Bandyopadhyay, A. Recent advances in bone tissue engineering scaffolds. Trends Biotechnol **30,** 546, 2012.
2. Mistry, A.S., and Mikos, A.G. Tissue engineering strategies for bone regeneration. Adv Biochem Eng Biotechnol **94,** 1, 2005.
3. Garg, T., and Goyal, A.K. Biomaterial-based scaffolds—current status and future directions. Expert Opin Drug Deliv **11,** 767, 2014.
4. Agarwal, R., and García, A.J. Biomaterial strategies for engineering implants for enhanced osseointegration and bone repair. Adv Drug Deliv Rev **94,** 53, 2015.
5. Roohani-Esfahani, S.I., Newman, P., and Zreiqat, H. Design and fabrication of 3D printed scaffolds with a mechanical strength comparable to cortical bone to repair large bone defects. Sci Rep **6,** 19468, 2016.
6. Roseti, L., Parisi, V., Petretta, M., *et al*. Scaffolds for bone tissue engineering: state of the art and new perspectives. Mater Sci Eng C **78,** 1246, 2017.
7. Chan, B.P., and Leong, K.W. Scaffolding in tissue engineering: general approaches and tissue-specific considerations. Eur Spine J **17,** 467, 2008.
8. Velasco, M.A., Narváez-Tovar, C.A., and Garzón-Alvarado, D.A. Design, materials, and mechanobiology of

biodegradable scaffolds for bone tissue engineering. Biomed Res Int **2015,** 729076, 2015.
9. Perez, R.A., and Mestres, G. Role of pore size and morphology in musculo-skeletal tissue regeneration. Mater Sci Eng C **61,** 922, 2016.
10. Karageorgiou, V., and Kaplan, D. Porosity of 3D biomaterial scaffolds and osteogenesis. Biomaterials **26,** 5474, 2005.
11. Hutmacher, D.W. Scaffolds in tissue engineering bone and cartilage. Biomaterials **21,** 2529, 2000.
12. Ergun, A., Yu, X., Valdevit, A., Ritter, A., and Kalyon, D.M. Radially and axially graded multizonal bone graft substitutes targeting critical-sized bone defects from polycaprolactone/hydroxyapatite/tricalcium phosphate. Tissue Eng Part A **18,** 2426, 2012.
13. Pompe, W., Worch, H., Epple, M., *et al*. Functionally graded materials for biomedical applications. Mater Sci Eng A **362,** 40, 2003.
14. Liu, H., Yang, L., Zhang, E., *et al*. Biomimetic tendon extracellular matrix composite gradient scaffold enhances ligament-to-bone junction reconstruction. Acta Biomater **56,** 129, 2017.
15. Gadjanski, I. Mimetic hierarchical approaches for osteochondral tissue engineering. Adv Exp Med Biol **1058,** 143, 2018.
16. Zhu, C., Pongkitwitoon, S., Qiu, J., Thomopoulos, S., and Xia, Y. Design and fabrication of a hierarchically structured scaffold for tendon-to-bone repair. Adv Mater **30,** e1707306, 2018.
17. Bracaglia, L.G., Smith, B.T., Watson, E., Arumugasaamy, N., Mikos, A.G., and Fisher, J.P. 3D printing for the design and fabrication of polymer-based gradient scaffolds. Acta Biomater **56,** 3, 2017.
18. Shanjani, Y., Pan, C.C., Elomaa, L., and Yang, Y. A novel bioprinting method and system for forming hybrid tissue engineering constructs. Biofabrication **7,** 045008, 2015.
19. Lee, P., Tran, K., Chang, W., *et al*. Bioactive polymeric scaffolds for osteochondral tissue engineering: in vitro evaluation of the effect of culture media on bone marrow stromal cells. Polym Adv Technol **26,** 2015, 1476.
20. Du, Y., Hancock, M.J., He, J., *et al*. Convection-driven generation of long-range material gradients. Biomaterials **31,** 2686, 2010.
21. Yin, R., Zhang, N., Wang, K., *et al*. Material design and photo-regulated hydrolytic degradation behavior of tissue engineering scaffolds fabricated via 3D fiber deposition. J Mater Chem B **5,** 329, 2017.
22. Seol, Y.J., Park, J.Y., Jung, J.W., *et al*. Improvement of bone regeneration capability of ceramic scaffolds by accelerated release of their calcium ions. Tissue Eng Part A **20,** 2840, 2014.
23. Hajiali, F., Tajbakhsh, S., and Shojaei, A. Fabrication and properties of polycaprolactone composites containing calcium phosphate-based ceramics and bioactive glasses in bone tissue engineering: a review. Polym Rev **58,** 164, 2018.
24. Borden, M., El-Amin, S.F., Attawia, M., and Laurencin, C.T. Structural and human cellular assessment of a novel microsphere-based tissue engineered scaffold for bone repair. Biomaterials **24,** 597, 2003.
25. Philippart, A., Boccaccini, A.R., Fleck, C., Schubert, D.W., and Roether, J.A. Toughening and functionalization of bioactive ceramic and glass bone scaffolds by biopolymer coatings and infiltration: a review of the last 5 years. Expert Rev Med Devices **12,** 93, 2015.
26. Ju, D., Han, L., Li, F., Chen, S., and Dong, L. Crystallization, mechanical properties, and enzymatic degradation of biodegradable poly(ε-caprolactone) composites with poly(lactic acid) fibers. Polym Compos **34,** 1745, 2013.
27. Trachtenberg, J.E., Placone, J.K., Smith, B.T., Fisher, J.P., and Mikos, A.G. Extrusion-based 3D printing of poly (propylene fumarate) scaffolds with hydroxyapatite gradients. J Biomater Sci Polym Ed **28,** 532, 2017.
28. Chu, B., Zhang, L., Qu, Y., *et al*. Synthesis, characterization and drug loading property of monomethoxy-poly(ethylene glycol)-poly(ε-caprolactone)-poly(D,L-lactide) (MPEG-PCLA) copolymers. Sci Rep **6,** 34069, 2016.
29. Hernández, A.R., Contreras, O.C., Acevedo, J.C., and Moreno, L.G.N. Poly(ε-caprolactone) degradation under acidic and alkaline conditions. Am J Polym Sci **3,** 70, 2013.
30. Turnbull, G., Clarke, J., Picard, F., *et al.* 3D bioactive composite scaffolds for bone tissue engineering. Bioact Mater **3,** 278, 2018.
31. Do, A.V., Khorsand, B., Geary, S.M., and Salem, A.K. 3D Printing of scaffolds for tissue regeneration applications. Adv Healthc Mater **4,** 1742, 2015.
32. Zhang, X., Chang, W., Lee, P., *et al*. Polymer-ceramic spiral structured scaffolds for bone tissue engineering: effect of hydroxyapatite composition on human fetal osteoblasts. PLoS One **9,** e85871, 2014.
33. Sadiasa, A., Nguyen, T.H., and Lee, B.T. In vitro and in vivo evaluation of porous PCL-PLLA 3D polymer scaffolds fabricated via salt leaching method for bone tissue engineering applications. J Biomater Sci Polym Ed **25,** 150, 2014.
34. Guo, T., Holzberg, T.R., Lim, C.G., *et al.* 3D printing PLGA: a quantitative examination of the effects of polymer composition and printing parameters on print resolution. Biofabrication **9,** 024101, 2017.
35. Kwon, D.Y., Park, J.H., Jang, S.H., *et al*. Bone regeneration by means of a three-dimensional printed scaffold in a rat cranial defect. J Tissue Eng Regen Med **12,** 516, 2018.
36. Trombetta, R., Inzana, J.A., Schwarz, E.M., Kates, S.L., and Awad, H.A. 3D printing of calcium phosphate ceramics for bone tissue engineering and drug delivery. Ann Biomed Eng **45,** 23, 2017.
37. Asa'ad, F., Pagni, G., Pilipchuk, S.P., Giannì, A.B., Giannobile, W.V., and Rasperini, G. 3D-Printed scaffolds and biomaterials: review of alveolar bone augmentation and periodontal regeneration applications. Int J Dent **2016,** 1239842, 2016.
38. Ozkan, S., Kalyon, D.M., and Yu, X. Functionally graded β-TCP/PCL nanocomposite scaffolds: in vitro evaluation with human fetal osteoblast cells for bone tissue engineering. J Biomed Mater Res A **92,** 1007, 2010.
39. Nyberg, E., Rindone, A., Dorafshar, A., and Grayson, W.L. Comparison of 3D-printed poly-ε-caprolactone scaffolds functionalized with tricalcium phosphate, hydroxyapatite, bio-oss, or decellularized bone matrix. Tissue Eng Part A **23,** 503, 2017.
40. Huang, B., Caetano, G., Vyas, C., Blaker, J.J., Diver, C., and Bártolo, P. Polymer-ceramic composite scaffolds: the effect of hydroxyapatite and β-tri-calcium phosphate. Materials **11,** 129, 2018.

41. Shor, L., Güçeri, S., Wen, X., Gandhi, M., and Sun, W. Fabrication of three-dimensional polycaprolactone/hydroxyapatite tissue scaffolds and osteoblast-scaffold interactions in vitro. Biomaterials **28,** 5291, 2007.
42. Gonçalves, E.M., Oliveira, F.J., Silva, R.F., *et al*. Three-dimensional printed PCL-hydroxyapatite scaffolds filled with CNTs for bone cell growth stimulation. J Biomed Mater Res B Appl Biomater **104,** 1210, 2016.
43. Lam, C.X.F., Savalani, M.M., Teoh, S.H., and Hutmacher, D.W. Dynamics of in vitro polymer degradation of polycaprolactone-based scaffolds: accelerated versus simulated physiological conditions. Biomed Mater **3,** 034108, 2008.
44. Díaz, E., Sandonis, I., and Valle, M.B. In vitro degradation of poly(caprolactone)/nHA composites. J Nanomater **2014,** 1, 2014.
45. Sheikh, Z., Abdallah, M.N., Hanafi, A.A., Misbahuddin, S., Rashid, H., and Glogauer, M. Mechanisms of in vivo degradation and resorption of calcium phosphate based biomaterials. Materials (Basel) **8,** 7913, 2015.
46. Yeo, A., Rai, B., Sju, E., Cheong, J.J., and Teoh, S.H. The degradation profile of novel, bioresorbable PCL–TCP scaffolds: an in vitro and in vivo study. J Biomed Mater Res **84A,** 208, 2008.
47. Lu, J., Descamps, M., Dejou, J., *et al*. The biodegradation mechanism of calcium phosphate biomaterials in bone. J Biomed Mater Res **63,** 408, 2002.

Address correspondence to:
Antonios G. Mikos, PhD
Department of Bioengineering, MS-142
BioScience Research Collaborative
Rice University
6500 Main Street
Houston, TX 77030

E-mail: mikos@rice.edu

Received: October 26, 2018
Accepted: November 12, 2018
Online Publication Date: December 27, 2018